Journal of Physics: Conference Series **2647** (2024) 202002 doi:10.1088/1742-6596/2647/20/202002

Prediction of Ground and Building Vibrations Induced by High-speed Trains using a 3D Coupled Numerical Model Based on a Spectral Element Analysis Code

Duo Feng[1], Roberto Paolucci[1], and Ilario Mazzieri[2]

[1]Department of Civil and Environmental Engineering, Politecnico di Milano, Piazza Leonardo da Vinci 32, 20133, Milan, Italy
[2]MOX-Modelling and Scientific Computing, Department of Mathematics, Politecnico di Milano, Piazza Leonardo da Vinci 32, 20133, Milan, Italy

E-mail: duo.feng@polimi.it

Abstract. Controlling the vibrations induced by high-speed trains on environmental infrastructures, especially buildings situated along railway tracks, is an essential demand and a challenging task. In order to accurately predict the dynamic response of the ground and adjacent buildings to railway-induced vibrations, we conduct numerical validation based on an existing in-situ model test in Portugal. This validation is done using the spectral element numerical code SPEED, developed at Politecnico di Milano, which considers a fully coupled 3D model of both the ground and building. The mechanical parameters of the track structure, modeled by the beam on elastic foundation, are obtained by iteratively calibrating the analytical dynamic receptance curve according to the experimental data. We use a multi-objective optimization-based method to estimate the equivalent rectangular sections of building structural components. The recorded dynamic vertical responses of the nearby ground and building slab under the excitation of 219 km/h moving trains are compared with the numerical results. Specific attention is paid to the frequency range that dominates the dynamic response of the building to discuss the accuracy of the results.

1. Introduction

Due to the high efficiency and abundant passenger capacity, railway transportation, especially High-speed Railway (HSR) networks, are becoming the ideal solution for meeting the travel demands arising from rapid urbanization in megacities worldwide. Despite these advantages, HSR also has its drawbacks. One of them is the higher construction cost compared to conventional railways. Moreover, it can cause more disturbances to nearby residents [1, 2] and potential damage to adjacent vulnerable buildings, such as historical architectures [3]. To address these issues, operating sectors must consider additional mitigating solutions along sensitive stretches. The dilemma can be attributed to the limited understanding of the multi-scale system, as the complexity of the interactions between different components poses significant challenges for quantitative investigation.

Train-induced environmental vibrations comprise ground motion and building vibration, with the former being typically high-frequency (at least up to 150 Hz) and greater when mainly

considering the area near the track structure [4]. However, researchers are more interested in the low-frequency vibrations (less than 30 Hz) primarily induced by train axle loads, as they are relevant to typical dwelling responses. Additionally, the response level inside buildings is more important than the ground one from the perspective of inhabitants' comfort.

Ground and track have a multi-layered structure with material properties that remain invariant along the track. As such, ground motion can be predicted in a simplified manner using (semi-)analytical methods such as transfer matrix [5], thin layer [6] or analytical layer [7] methods. However, incorporating buildings into the track-ground system makes it a fully 3D and multi-scale problem due to the geometrical and mechanical differences between the components. Simplified substructuring and multi-stage numerical methods such as MBS-FEM [8] and 2.5D-3D FEM [9] are therefore increasingly used. Nevertheless, accurately investigating the influence of ground on structural vibrations under train passages, and vice versa, is still quite challenging.

Recently, the hybrid method, which reduces the prediction uncertainties through dedicated tests and validated numerical results [10], has become increasingly popular in scoping predictions [11]. However, advanced numerical methods are more attractive because they allow coupled analyses to be carried out. For instance, it has been demonstrated that the spectral element method could offer higher accuracy and efficiency even in the analysis of seismic soil-city interaction [12, 13, 14]. Moreover, this method was used to successfully investigate the qualitative impact of three urban railway types on ground and building vibration [15].

In order to investigate this phenomenon more quantitatively, a numerical validation of a coupled 3D spectral element model with other methods is conducted to predict train-induced ground and building vibration. This is based on an existing well-conducted building model field test in Portugal [16]. The quality of the numerical results and the possible reasons for discrepancies in the low-frequency range are analyzed in comparison with the test records.

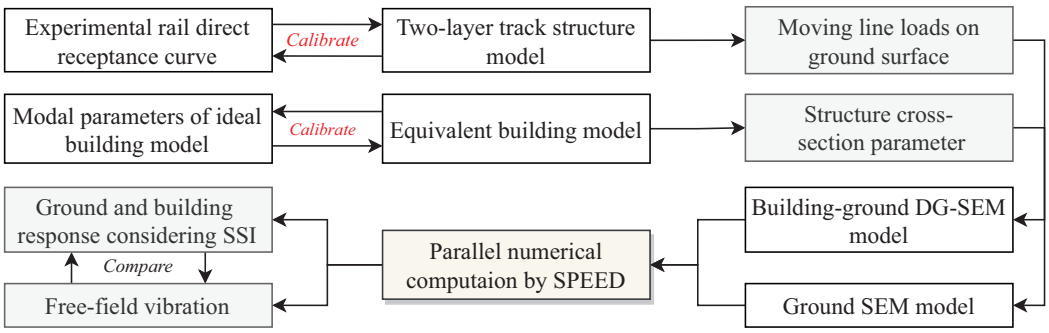

Figure 1. Flowchart for predicting train-induced environmental vibrations using coupled SEM model.

2. Prediction methodology

To reduce the prediction discrepancies caused by the material parameter uncertainties, in this study most of the dynamic properties of the track and building were calibrated based on related tests, as shown in Figure 1.

2.1. Decoupled train-embankment dynamic model

As mentioned previously, the focus of this study is on the frequency range associated with building vibrations. Interactions between the rough rail and wheel with dominant frequencies greater than 100 Hz can be neglected. Therefore, to obtain the stress field of ground surface under the track structure, a continuous two-layer elastic foundation model is utilized, which is subjected to a series of moving axle loads. To accurately model the track-ground system, the

coefficients of the track components need to be calibrated using receptance test results through a prior optimization process.

The two-layer elastic foundation model, illustrated in Figure 2(a), is used to describe the low-frequency responses of the ballast track. The dynamic characteristics of each component are defined by the following differential equations in the general Cartesian coordinate system (shown in Figure 2(a)) when a sinusoidal point load is applied to the sleeper

$$\begin{aligned} m_r \frac{\partial^2 u_1}{\partial t^2} + EI \frac{\partial^4 u_1}{\partial x^4} &= -\left(k_p + c_p \frac{\partial}{\partial t}\right)(u_1 - u_2), \\ m_s \frac{\partial^2 u_2}{\partial t^2} &= \left(k_p + c_p \frac{\partial}{\partial t}\right)(u_1 - u_2) - \left(k_b + c_b \frac{\partial}{\partial t}\right) u_2 + P e^{\mathrm{i}\omega_0 t} \delta(x). \end{aligned} \tag{1}$$

The equations consist of various parameters, including m_r and EI representing the rail's unit mass and bending stiffness, respectively, and k_p and c_p denoting the unit linear stiffness and damping coefficient of the rail pads. The calibration of these five parameters is based on the manufacturer's provided values [17].

Additionally, m_s, k_b and c_b represent the unit mass, stiffness, and damping coefficient of the ballast-embankment system, respectively. The vertical displacement of the rail and sleepers are represented by u_1 and u_2, respectively, and they are both functions of the longitudinal coordinate x and time t. Finally, P and ω_0 denote the amplitude and angular frequency of the harmonic point load, respectively, while the load's location is defined by the Dirac function $\delta(\cdot)$. For convenience, introduce the characteristic length $L = EI\,(k_p + k_b)/(k_p k_b)$.

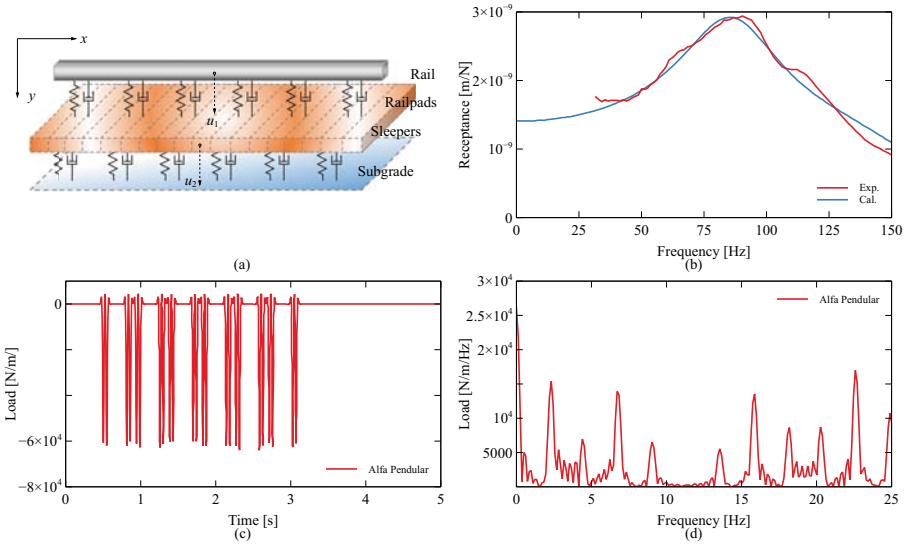

Figure 2. (a) Two-layer elastic foundation model; (b) comparison of experimental/numerical cross rail receptance; distribution of train loads on the ground surface in time (c) and frequency (d) domain.

The equations are solved simultaneously using the integral transform method, where s represents the transformed variable of x as derived in [18]. The steady-state rail cross receptance, considering the sleeper interval l, is expressed as a summation form of residuals

$$\alpha(\omega_0) = \sum_{k=1}^{2} \mathrm{i}\,\mathrm{Res}\left(\frac{-F_p \exp(\mathrm{i}s_k l)}{L\left[F_p^2 - (F_p + F_r)(F_b + F_p + F_s)\right]}\right)\Bigg|_{\mathrm{Im}(s_k)>0}, \tag{2}$$

and

$$\begin{aligned} F_p\left(k_p, c_p, \omega_0\right) = k_p + c_p \mathrm{i}\omega_0, F_b\left(k_b, c_b, \omega_0\right) = k_b + c_b \mathrm{i}\omega_0, \\ F_s\left(m_s, \omega_0\right) = -m_s\omega_0^2, F_r\left(EI, L, m_r, \omega_0, s_k\right) = EIs_k^4/L^4 - m_r\omega_0^2. \end{aligned} \tag{3}$$

The values of the parameters k_b, c_b, and m_s can be determined using a general optimizing method by fitting the test receptance records $\alpha_e(\omega_0)$ in the concerned frequency band. The method uses a least squares objective function, which minimizes the sum of squares of the differences between the measured and calculated receptance values. The objective function can be expressed as $\min : \sum \left(\alpha\left(\omega_{(0,i)}\right) - \alpha_e\left(\omega_{(0,i)}\right)\right)^2$. The calibrated values are listed in Table 1. Figure 2(b) displays the cross rail receptance resulting from the calibrated coefficients, compared with the test results. The comparison illustrates that the dynamic properties of the track structure can be reasonably reproduced.

Table 1. Material parameters of components in two-layer elastic foundation model

Component	Parameter	Value
Rail	m_r [kg/m]	60
	EI [Nm^2]	6.42×10^6
Railpad	k_p [N/m^2]	1.03×10^9
	c_p [Ns/m^2]	37500
Sleeper-embankment	m_s [kg/m]	1.36×10^3
	k_b [N/m^2]	4.30×10^8
	c_b [Ns/m^2]	3.50×10^5

Furthermore, the moving line load on the ground surface can be determined by the steady-state solution of the track model under a series of moving axle loads in the moving coordinate system. It's assumed that the rail and sleeper displacement responses, as well as the moving point load, have the following Fourier series expansion [19]

$$\begin{aligned} u_1(\xi) &= \frac{u_{1,0}}{2} + \sum_{i=1}^{+\infty} A_i \cos\Omega_i\xi + B_i \sin\Omega_i\xi, \\ u_2(\xi) &= \frac{u_{2,0}}{2} + \sum_{i=1}^{+\infty} C_i \cos\Omega_i\xi + D_i \sin\Omega_i\xi, \\ P(\xi) &= \frac{Q}{\lambda} + \sum_{i=1}^{+\infty} \frac{2Q}{\pi p i}\left[\sin\pi i - \sin\left(\pi i - \pi i p/\lambda\right)\right]\cos\Omega_i\xi, \quad \left(\Omega_i = 2\pi i/\lambda\right), \end{aligned} \tag{4}$$

where the variable Q represents the magnitude of the axle load, and p denotes the width of the equivalent rectangular load used to simulate the rail-wheel contact area. The constant λ denotes the effective influential length of one single axle load, while $\xi = x - vt$ represents the horizontal coordinate moving at velocity v.

The steady-state moving loads $F_t(x,t)$ on the ground surface caused by the passage of train vehicles can be obtained by summing up the components induced by n axle loads.

$$F_t(x,t) = F_t(\xi) = F_t(x - vt) = \sum_{i=1}^{n} F_{t,i}(x - vt) = \sum_{i=1}^{n} k_b u_{2,i}(x - vt) \tag{5}$$

The unknown coefficients A_i to D_i can be obtained by simultaneously solving Equations (1) and (4). The convergence of the result is achieved when the number of series exceeds 2000, based on several attempts made by the authors.

2.2. Coupled ground-building dynamic model

This research employed the fully coupled soil-structure dynamic analysis achieved by using the Spectral Element Method (SEM) through SPEED, an high-performance open-source numerical code [12]. Since SPEED is primarily designed for seismic wave propagation studies related to earthquake engineering, some aspects of the modeling require careful attention in this application.

Joint faces between the footings and the ground are crucial for a general conforming mesh modeling, particularly when the building adopts shallow foundations. Such analysis requires a significant number of elements, which may still pose risks of mesh qualities. To address this challenge, this paper employs a Discontinuous Galerkin (DG) spectral formulation to construct a non-conforming hexahedral mesh, which is embedded in SPEED.

The responses of receivers such as beams and slabs are mainly governed by their flexural performances under the moving high-speed trains. Therefore, to reduce the effects of shear locking, higher-order interpolating polynomials are recommended. The value of all bending structures in this study is set at 2.

To minimize the inefficiency caused by the minimal solid element length, an equivalent building model was estimated through iterative optimization, compared to the actual model, to retain most vertical dynamic properties in the interested frequency domain.

3. Test stretch

3.1. Location

The experimental site is located in Carregado, which is a part of the Portuguese railway network connecting Lisbon and Porto. Due to its characteristic hybrid operation with several types of vehicles, numerous tests have been conducted, resulting in a wealth of data, which has made it a benchmark test in this field [17].

The high-speed train Alfa Pendular, which consists of six carriages and has a total length of 158.9 m, operates at speeds of up to 220 km/h. The specific axle loads and wheel intervals are listed in [17]. Figure 2(c) and (d) show the characteristics of the moving line distributed loads on the ground surface, which were obtained following the methods described in Section 2.1 and are presented in terms of time history and Fourier spectrum.

Table 2. Profiles and mechanical parameters of soil. (the values in the mass density column represent the estimated values based on SPT results [20], as well as the values used in the simulation.)

Layer	Thickness [m]	N_{SPT}	ρ [kg/m^3]	C_s [m/s]	C_p [m/s]	η
1	2.00	4	1551.83 (1500)	118.00	410.00	0.08
2	2.00	13	1634.43 (1600)	118.00	1072.00	0.04
3	4.00	18	1658.00 (1600)	118.00	1072.00	0.03
4	4.00	15	1964.64 (1900)	212.00	1503.00	0.03
5	31.5	15	1964.64 (1900)	302.00	1503.00	0.03

3.2. Soil profile

The soil profile and mechanical properties at the site were determined using the cross-hole and SASW tests to accommodate the general and train-induced vibration level. The soil wave velocity and other material parameters are summarized in Table 2. It is worth noting that the groundwater level is located at a depth of approximately 4 meters.

3.3. Building parameters

A three-story framed structure, scaled at 1:3 and supported by four individual footings, was constructed 21.2 m away from the center of the track. The natural frequencies of floor slabs made of medium density fiberboard are in the range of 15 to 20 Hz. The edges of the slabs and the bottoms of the columns were bolted to limit all degrees of freedom. The profiles and material properties of the building model are detailed in Table 3.

Table 3. Building material and profile properties

Components	ρ [kg/m^3]	C_p [m/s]	C_s [m/s]	η	Profiles and dimensions [m]	
					Actual ones	Equivalent ones
Beam	7850	6000.00	3207.66	0.01	IPE 100	0.057/0.024
Pillar						0.093/0.067
Footing	2500	3740.23	2290.41	0.01	0.7×0.7×0.35	—
Slab	700	2618.61	1511.86	0.01	2.1×2.1×0.03	

3.4. Monitoring details

Before constructing the small-scale building model, accelerometers were installed along a straight line perpendicular to the direction of railway to record the ground response induced by the Alfa Pendular. The farthest sensor used in this study was located 22.5 m away from the railway, which is almost the same position as the framework. After the construction of the building model, more efforts were made to focus on the structure. Accelerometers were vertically fixed on the floor slabs and around the footings. The location distribution and coordinates of monitoring points are shown in Table 4 and represented by colored spheres in Figure 4(b). For more detailed information, please refer to [16].

Table 4. The coordinates of monitoring points

Points	Coordinates [m]	Location
S0	(0.0, 9.20, 0.0)	Ground surface
S1	(0.0, 15.0, 0.0)	
S2	(0.0, 22.5, 0.0)	
S3	(-3.5, 17.7, 0.0)	
M1	(2.2, 20.1, 0.0)	Floor slab
P2	(0.0, 21.2, 2.0)	
P21	(0.5, 20.7, 2.0)	

4. Numerical modeling and validation

4.1. Numerical parameter calibration

Apart from track structure parameters, the building geometric parameters are calibrated towards an equivalent model. Figure 3(a) illustrates the modal frequency analysis results of the fixed-base building. In terms of three directional modal mass ratio distribution, Figure 3(b) displays the key role of floor slabs' flexural modes dominating building vertical responses, horizontal vibrations are however controlled by the first two modes of pillars.

The equivalent building model using solid elements is expected to have similar modal parameters as the actual one. Moreover, the calibration strategy is based on an optimization procedure in which structural cross-sectional parameters are modified. Equation (6) shows the

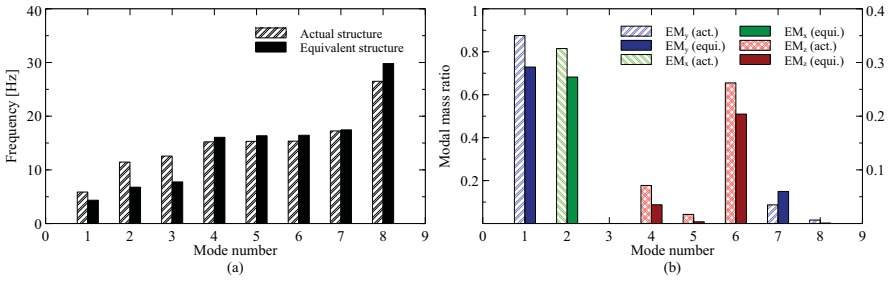

Figure 3. Modal parameters calibration: (a) the natural frequencies of first eight mode of the actual and equivalent structures; (b) the modal mass ratios of the actual and equivalent structures. (components related to the z direction refer to the right y axis, the others refer to the axis on the left side.)

objective function associated with dynamic and static properties. It is equally important to note that building profiles, such as the longitudinal lengths of beams and pillars, remain unchangeable during the iterations.

$$\begin{aligned} \min_{a_1,b_1,a_2,b_2} \quad & \sum_{i=1}^{8} |f_{e,i} - f_i| + |m_{e,i}/M_e - m_i/M| + |\Delta_{\max,e} - \Delta_{\max}|\,, \\ \text{s.t.} \quad & a_j \in [0.75a_{j,0},\ 1.25a_{j,0}],\ (j = 1,\ 2), \\ & b_k \in [0.75b_{k,0},\ 1.25b_{k,0}],\ (k = 1,\ 2), \end{aligned} \tag{6}$$

where a_1 to b_2 represent the geometric parameters of rectangular sections of beams or pillars, with $a_{j,0}$ and $b_{k,0}$ representing the default values. The eigenfrequencies and modal mass ratios are denoted by f and m/M, respectively. Additionally, $\Delta_{\max}$ is the maximum deflection of the third-floor slab subjected to a unit vertical point load at the center of the slab.

The computation was carried out for approximately five hours using Isight with ABAQUS by the Pointer algorithm. The calibrated section parameters are presented in Table 3, and the related modal parameters are displayed in Figure 3, indicating an acceptable agreement with the actual values.

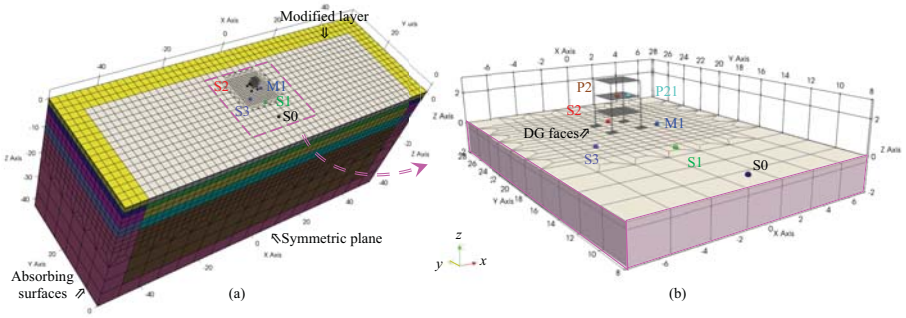

Figure 4. (a) Ground-building coupled DG-SE model; (b) Monitoring points locations.

During the modeling process, symmetric boundary conditions were applied along the middle plane between the two rails to reduce computational consumption. To avoid numerical divergences caused by the accuracy limitations of paraxial boundary conditions applied to soil with a Poisson's ratio approaching 0.5, the compressive wave velocity of the soil near the border is adjusted to achieve a Poisson's ratio of 0.25.

The element sizes follow the grid dispersion condition, with a maximum value of $l_{e,i} = C_{p,i}/(f_{\max}G)$, where G is 4 for spectral elements and $f_{\max} = 28$ Hz is used to investigate the

activated structural modes. Figure 4(a) shows the coupled building-ground SE model, which has a longitudinal length of 100 m.

4.2. Free-field vibration prediction and comparison

To avoid response singularity issues caused by line loads, accelerometers located outside of the embankment area were selected. Figure 5 shows the time and frequency domain vertical velocity responses of two monitoring points, S1 and S2, located at distances of 15 m and 22.5 m from the track center, respectively.

Despite the frequency component distributions are similar to the experimental ones, the predicted velocity amplitudes show relatively weak agreement in the high frequency range. This is likely more due to the complexity of the damping properties of the soil than the influence of dynamic axle loads being disregarded. The soil property tests and the train excitation experiments were conducted during the different seasons [17]. Hence, variations in the water level could influence parameter calibration. Additionally, the numerical frequency components slightly shift to the left, suggesting that the actual velocity of the moving trains may be higher than the measured value.

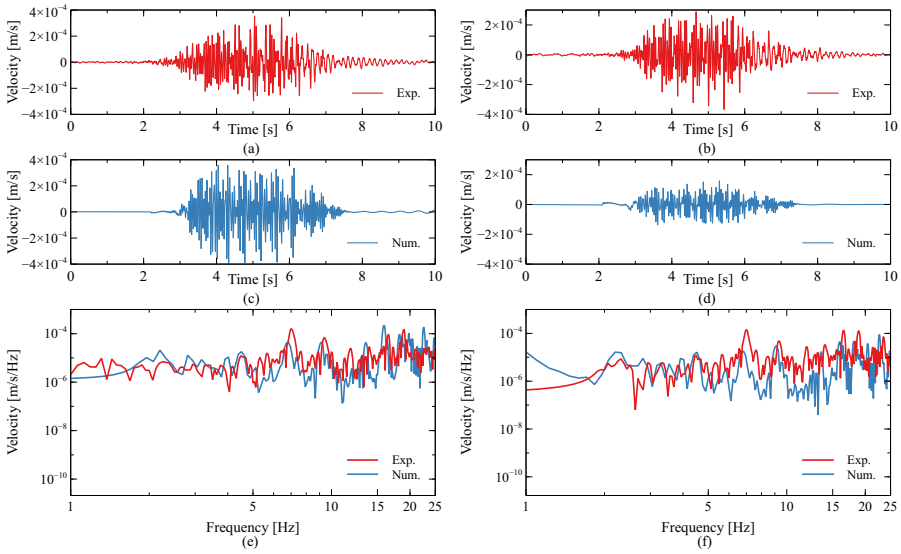

Figure 5. Comparison of experimental/numerical free-field vertical velocity responses, left side: S1 and right side: S2 (15 m and 22.5 m away from the railway center) in time and frequency domains.

4.3. Building-ground vibration and comparison

Figure 6 compares the predicted and experimental velocity responses of two measuring points, P2 and P21, on the slabs in the time and frequency domains. The numerical results adequately capture the main features of slab vibrations. However, in contrast to the free-field cases, The minor shifts in frequency components can be attributed to the inaccurate calibration of the equivalent cross sections in Section 4.1, which has also resulted in shorter response durations. Furthermore, the two frequency peaks are identified as the bending modes of the slab with decreased eigenfrequencies due to the effect of ground absorption.

Figure 7(a), (d) and (g) show the responses of M1, which is located 1 m away from the building footing, with and without considering the building's presence. The numerical results agree well with the test results in time history. To demonstrate clearly, the results in frequency domain are processed to Root Mean Square (RMS)-based values in 1/3 octave band. Although

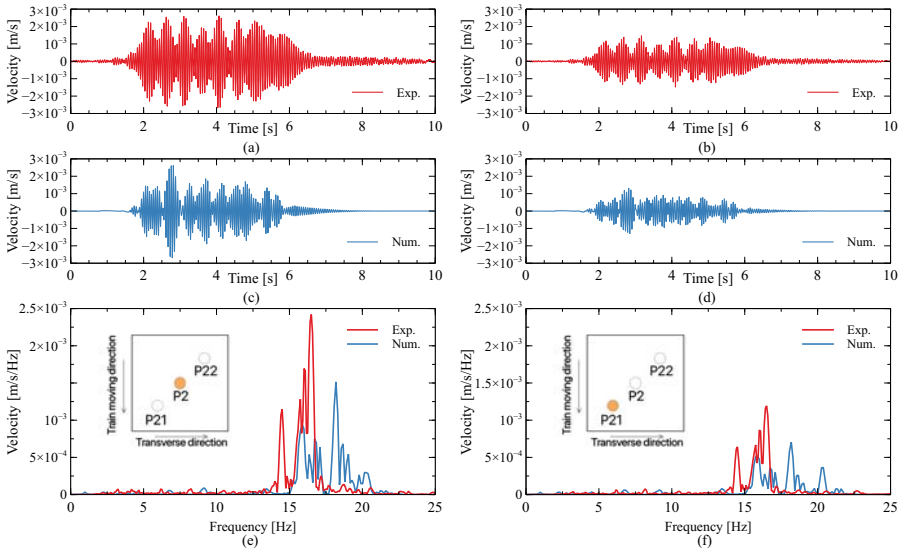

Figure 6. Comparison of experimental/numerical vertical velocity responses, left side: P2 and right side: P21 on the second-floor slab in time and frequency domains (the sensors locations on the slab are shown in the embedded diagrams in (e) and (f)).

the distribution of the numerical frequency components does not match the experimental ones locally, the responses that consider the building construction are larger than those without considering it in the high-frequency range. This indicates the effect of the vibration of the structural component like the floor slabs.

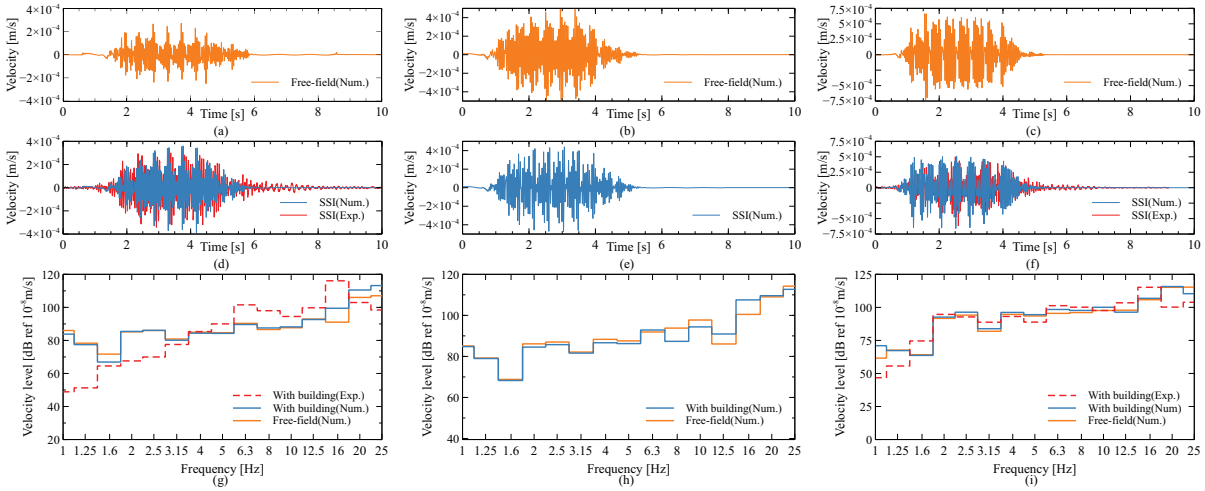

Figure 7. Comparison of vertical experimental/numerical velocity responses of points whether or not considering the impact of added-building. Left side: M1 (1 m away from footings); middle side: S3 (3 m away from footings); right side: S0 (12 m away from footings) in time and frequency domains.

This effect is even more obvious for the ground response of S3, which is located further away from M1, as shown in Figure 7(b), (e) and (h). In other words, interferences may occur between the building and the nearby ground. This effect is less pronounced for distant points like S0, which is located 12 m outside the building, as illustrated in Figure 7(c), (f) and (i). There is good agreement between the predicted and actual results in both the time and frequency

domains. This may be due to the decreasing effect of building resonance.

5. Conclusions

(1) The proposed strategy for the estimation of equivalent cross-sectional dimensions of building components based on modal parameters improves the efficiency of the numerical methods using solid elements for the analysis of environmental vibration induced by fast trains;

(2) The spectral element method combined with the two-layer elastic foundation model shows the promising capability of simulating most of properties of the fast train-induced ground and building vibrations both in time and frequency domains;

(3) In this particular in-situ model test, the presence of the building likely amplifies the vibration of the area adjacent to the footings, especially in the frequency range that covers the bending modes of floor slabs.

Acknowledgments

This research and the first author's study are supported by the China Scholarship Council (Grant No. 202106370077). The numerical calculations were carried out using the G100 HPC at CINECA, under project reference "ISCRA B SSI-RISK". The authors would also like to express their sincere gratitude to Prof. Aires Colaço for kindly providing the comprehensive test data of the Carregado experiment.

References

[1] Waye K P, Li H, van Kempen E, Ögren M and Vincens N 2022 *proceedings of the 24th International Congress on Acoustics*
[2] Jik Lee P and Griffin M J 2013 *The Journal of the Acoustical Society of America* **133** 2126–2135
[3] Erkal A, Laefer D, Fanning P, Durukal E, Hancilar U and Kaya Y 2010 *Advanced Materials Research* vol 133 (Trans Tech Publ) pp 569–574
[4] Knothe K and Grassie S 1993 *Vehicle system dynamics* **22** 209–262
[5] Sheng X z, Jones C and Petyt M 1999 *Journal of sound and vibration* **228** 129–156
[6] Jones S and Hunt H 2011 *Journal of engineering mechanics* **137** 887–900
[7] Zhenning B, Liang J, Lee V W and Gao Y 2019 *Soil Dynamics and Earthquake Engineering* **121** 25–39
[8] Qu S, Yang J, Zhu S, Zhai W and Kouroussis G 2021 *Transportation Geotechnics* **31** 100682
[9] Colaço A, Costa P A, Amado-Mendes P and Calçada R 2021 *Engineering Structures* **240** 112381
[10] Hanson C E, Ross J C, Towers D A, Harris M *et al.* 2012 High-speed ground transportation noise and vibration impact assessment. Tech. rep. United States. Federal Railroad Administration. Office of Railroad Policy ...
[11] Kuo K, Papadopoulos M, Lombaert G and Degrande G 2019 *Journal of Sound and Vibration* **442** 459–481
[12] Mazzieri I, Stupazzini M, Guidotti R and Smerzini C 2013 *International Journal for Numerical Methods in Engineering* **95** 991–1010
[13] Lu X, Tian Y, Wang G and Huang D 2018 *Earthquake Engineering & Structural Dynamics* **47** 2708–2725
[14] Kato B and Wang G 2022 *Bulletin of Earthquake Engineering* **20** 1431–1454
[15] Stupazzini M and Paolucci R 2010 *ISMA2010 International Conference on Noise and Vibration Engineering* pp 20–22
[16] Colaço A, Costa P A, Castanheira-Pinto A, Amado-Mendes P and Calçada R 2021 *Soil Dynamics and Earthquake Engineering* **141** 106499
[17] Dos Santos N C, Colaço A, Costa P A and Calçada R 2016 *Soil Dynamics and Earthquake Engineering* **90** 358–380
[18] Grassie S, Gregory R, Harrison D and Johnson K 1982 *Journal of Mechanical Engineering Science* **24** 77–90
[19] Czyczula W, Koziol P, Kudla D and Lisowski S 2017 *Journal of Vibration and Control* **23** 2989–3006
[20] Anbazhagan P, Uday A, Moustafa S S and Al-Arifi N S 2016 *Journal of Geophysics and Engineering* **13** 320–341